Author/s:
Hooijmans, MT;Froeling, M;Koeks, Z;Verschuuren, JJGM;Webb, A;Niks, EH;Kan, HE

Title:
Multi-parametric MR in Becker muscular dystrophy patients

Date:
2020-11-01

Citation:
Hooijmans, M. T., Froeling, M., Koeks, Z., Verschuuren, J. J. G. M., Webb, A., Niks, E. H. & Kan, H. E. (2020). Multi-parametric MR in Becker muscular dystrophy patients. NMR in Biomedicine, 33 (11), pp.e4385-. https://doi.org/10.1002/nbm.4385.

Persistent Link:
https://hdl.handle.net/11343/277792

Received: 17 November 2019 | Revised: 9 July 2020 | Accepted: 13 July 2020

DOI: 10.1002/nbm.4385

RESEARCH ARTICLE

NMR IN BIOMEDICINE WILEY

Multi-parametric MR in Becker muscular dystrophy patients

Melissa T. Hooijmans[1,2] | Martijn Froeling[3] | Zaida Koeks[4] | Jan J.G.M. Verschuuren[4,5] | Andrew Webb[1] | Erik H. Niks[4,5] | Hermien E. Kan[1,5]

[1]C.J. Gorter Center, Department of Radiology, Leiden University Medical Center, Leiden, The Netherlands

[2]Department of Biomedical Engineering & Physics, Amsterdam University Medical Centers, Amsterdam, The Netherlands

[3]Department of Radiology, Utrecht University Medical Center, Utrecht, The Netherlands

[4]Department of Neurology, Leiden University Medical Center, Leiden, The Netherlands

[5]Duchenne Center Netherlands, The Netherlands

Correspondence
M.T. Hooijmans, Department of Biomedical Engineering & Physics, Z0-174, A UMC, Meibergdreef 9, 1105 AZ Amsterdam, The Netherlands
Email: m.t.hooijmans@amsterdamumc.nl

Funding information
The Netherlands Organization for Health Research and Development, Grant/Award Number: 113302001

Quantitative MRI and MRS of muscle are increasingly being used to measure individual pathophysiological processes in Becker muscular dystrophy (BMD). In particular, muscle fat fraction was shown to be highly associated with functional tests in BMD. However, the muscle strength per unit of contractile cross-sectional area is lower in patients with BMD compared with healthy controls. This suggests that the quality of the non-fat-replaced (NFR) muscle tissue is lower than in healthy controls. Consequently, a measure that reflects changes in muscle tissue itself is needed. Here, we explore the potential of water T_2 relaxation times, diffusion parameters and phosphorus metabolic indices as early disease markers in patients with BMD. For this purpose, we examined these measures in fat-replaced (FR) and NFR lower leg muscles in patients with BMD and compared these values with those in healthy controls. Quantitative proton MRI (three-point Dixon, multi-spin-echo and diffusion-weighted spin-echo echo planar imaging) and 2D chemical shift imaging ^{31}P MRS data were acquired in 24 patients with BMD (age 18.8-66.2 years) and 13 healthy controls (age 21.3-63.6 years). Muscle fat fractions, phosphorus metabolic indices, and averages and standard deviations (SDs) of the water T_2 relaxation times and diffusion tensor imaging (DTI) parameters were assessed in six individual leg muscles. Phosphodiester levels were increased in the NFR and FR tibialis anterior, FR peroneus and FR gastrocnemius lateralis muscles. No clear pattern was visible for the other metabolic indices. Increased T_2 SD was found in the majority of FR muscles compared with NFR and healthy control muscles. No differences in average water T_2 relaxation times or DTI indices were found between groups. Overall, our results indicate that primarily muscles that are further along in the disease process showed increases in T_2 heterogeneity and changes in some metabolic indices. No clear differences were found for the DTI indices between groups.

Abbreviations: ATP, adenosine triphosphate; BMD, Becker muscular dystrophy; cCSA, contractile cross-sectional area; CSI, chemical shift imaging; DMD, Duchenne muscular dystrophy; DTI, diffusion tensor imaging; EPG, extended phase graph; EPI, echo planar imaging; FA, fractional anisotropy; FOV, field of view; FR, fat replaced; GCL, gastrocnemius lateralis muscle; GCM, gastrocnemius medialis muscle; GRMD, Golden Retriever muscular dystrophy; MD, mean diffusivity; MSME, multi-slice multi-echo; NFR, non-fat-replaced; NSA, number of signal averages; PCr, phosphocreatine; PDE, phosphodiester; PER, peroneus muscle; P_i, inorganic phosphate; ROI, region of interest; RP, spectrally selective fat suppression; SD, standard deviation; SE, spin echo; SI, signal intensity; SNR, signal-to-noise ratio; SOL, soleus muscle; SPAIR, spectrally adiabatic inversion recovery; SSGR, slice-selection gradient reversal; qT2, quantitativeT_2; TA, anterior tibialis muscle; TP, posterior tibialis muscle; λ_1, Eigenvalue 1; λ_2, Eigenvalue 2; λ_3, Eigenvalue 3.

KEYWORDS
Becker muscular dystrophy, phosphorus MRS, quantitative MRI, skeletal muscle

1 | INTRODUCTION

Becker muscular dystrophy (BMD) is an X-linked disease caused by a mutation in the *DMD* gene, which codes for the protein dystrophin. Dystrophin in muscle anchors the contractile apparatus to the surface membrane to ensure membrane stability during muscle contractions.[1] The dystrophin protein in patients with BMD is truncated, and therefore its function is impaired, which manifests itself in on-going muscle fiber damage and muscle weakness.[2,3] This muscle fiber damage is reflected by a variety of processes such as changes in energy metabolism, muscle fiber size, inflammation, fibrosis and replacement of muscle tissue by fat.[2,3]

Quantitative MRI (qMRI) and MRS are increasingly used to measure these individual pathophysiological processes in muscular dystrophies, including BMD.[4–7] In particular, the muscle fat fraction measured with MR is frequently used and has been shown to be highly associated with functional measures such as 6 min walking distance, time-graded tests and muscle force measurements in BMD.[6–9] Another measure increasingly used in neuromuscular disease and thought to be closely associated with muscle function is contractile cross-sectional area (cCSA). This measure can be derived from the fat fraction in combination with muscle volume and represents the remaining muscle tissue ((1 − fat fraction) × muscle volume = cCSA).[10] Interestingly, previous work showed that the cCSA does not correlate with muscle function in BMD, and that this correlation is weaker in the more severely affected Duchenne muscular dystrophy (DMD) patients (dystrophin is fully absent) compared with healthy age-matched controls. This indicates that the functionality of the non-fat-replaced (NFR) muscle tissue in these patients groups is lower than in healthy controls.[7,10] Therefore, non-invasive outcome measures that reflect changes in the muscle tissue itself are needed.

One of such measures is phosphodiester (PDE) levels detected with ^{31}P MRS. The PDE signal in the MR spectrum is derived from glycerol 3-phosphocholine (GPC) and glycerol 3-phosphoethanolamine (GPE), which are thought to be membrane phospholipid breakdown products. In diseases with muscle wasting, such as DMD and BMD, the membrane damage is hypothesized to result in an increase in PDE. Previous work showed that, in both patients with BMD and patients with DMD, PDE levels were higher in muscles without fat replacement.[11,12] Another candidate MR-related technique is diffusion tensor imaging (DTI), which produces measures sensitive to microstructural changes in muscle injury and microtrauma and after exercise.[13,14] DTI applications in neuromuscular diseases are limited due to the challenges posed by fat replacement.[15,16] However, simulation work and in vivo studies have shown that DTI indices can be reliably estimated when these confounding factors are accounted for.[17–19] Finally, the average water T_2 relaxation times and T_2 heterogeneity assessed via quantitative T_2 (qT2) mapping could be useful early markers, as both the average and standard deviation (SD) of water T_2 values have been shown to be sensitive to inflammatory processes and disease activity in neuromuscular diseases.[20,21] Water T_2 relaxation times are commonly measured in neuromuscular diseases but have only been rarely investigated in patients with BMD: these studies showed similar or only slightly elevated water T_2 relaxation times compared with healthy controls.[22,23] Both DTI indices and PDE levels have been associated with membrane integrity in skeletal muscle.[13,24,25] However, little is known about the relation between these measures since these outcome measures have not been assessed together.

Therefore the primary aim of this work is to explore the potential of water T_2 relaxation times, diffusion indices and phosphorus metabolic indices as early disease markers in patients with BMD, by examining these measures in fat-replaced (FR) and NFR lower leg muscles in comparison with values in healthy controls. As both DTI indices and PDE levels have been associated with changes in membrane integrity in skeletal muscle, we also aimed to investigate the relation between PDE levels and DTI indices using a correlation analysis.

2 | METHODS

2.1 | Patient population

A total of 24 male patients with BMD (age 42.9 ± 13.05; range 18.8-66.2 yr) and 13 male healthy control subjects (age 43 ± 13.68; range 21.3-63.6 yr) participated in the study. Patients with BMD were recruited from the Dutch Dystrophinopathy Database.[26] All diagnoses were confirmed by a mutation in the DMD gene. All patients with BMD were ambulant (defined as being able to walk 10 m with the support of a walking aid). Of the 24 patients with BMD, 12 patients with BMD had participated in our previously-published MR studies.[11,22] The study was approved by the local medical ethical committee and all patients signed informed consent.

2.2 | MR examination at 3 T

Data were acquired in the lower leg on a 3T MR system (Philips Ingenia, Best, The Netherlands) with a 16-element receive coil placed on the anterior section of the leg and the 12-element coil built into the patient table positioned posterior to the leg. Subjects were positioned in a feet-first supine position in the scanner. The imaging protocol consisted of five sequences.

I. Spin-echo (SE)-Echo Planar Imaging (EPI) DTI sequence to obtain diffusion indices (T_R/T_E 2990/49 ms; number of signal averages (NSA) 6; number of gradient directions 16; *b*-values 0, 450 s/mm^2; voxel size 2 × 2 × 6 mm^3; 12 slices; no gap). A combination of three techniques was used to suppress the fat signal[15]: a spectrally adiabatic inversion recovery (SPAIR) pulse and slice-selection gradient reversal (SSGR) for the aliphatic fat peak and a spectrally selective fat suppression (RP) pulse for the olefinic fat peak).
II. SE-EPI without diffusion weighting to assess the signal-to-noise ratio (SNR) (T_R/T_E 3020/49 ms; NSA 6; *b*-value 0 s/mm^2; voxel size 2 × 2 × 6 mm^3; 12 slices; no gap; 10 dynamics; SPAIR; SSGR; RP).
III. T_1-weighted sequence used as anatomical reference for the DTI (T_R/T_E 630/30 ms; voxel size 1.5 × 1.5 × 6 mm^3; no gap, 12 slices).
IV. Three-point Dixon sequence to determine muscle fat fraction levels ($T_R/T_E/\Delta T_E$ 210/4.41/0.76 ms; NSA 2; flip angle 8°; voxel size 1 × 1 × 10 mm^3; slice gap 5 mm; 23 slices).
V. Multi-echo multi-slice (MEMS) sequence to measure water T_2 relaxation times (17 echoes; $T_R/T_E/\Delta T_E$ 3000/8/8 ms; voxel size 1.4 × 1.8 × 10 mm^3; slice gap 20 mm; 5 slices).

The middle of the slice stack for all five sequences was aligned and positioned at the thickest part of the calf and perpendicular to the tibia bone.

2.3 | MR examination at 7 T

On the same day as the 3T scans, ^{31}P MRS datasets were acquired on a 7T MR system (Philips Achieva) with a custom-built double tuned (^{31}P and ^{1}H) volume coil (length 12 cm). The coil was placed at the thickest part of the calf just below the patella, to ensure accurate co-localization with the MR measurements at 3T. The imaging protocol consisted of the following.

I. ^{31}P 2D chemical shift imaging (CSI) scan to assess phosphorus metabolic indices (Field of View (FOV) 160 × 200; matrix size 8 × 10; T_R 2000 ms; 2048 complex data points). Excitation was performed with a block pulse with individually determined flip angle of 45° using a flip angle series prior to the CSI acquisition. The acquisition was Hamming weighted with 24 signal averages of the central *k*-lines.
II. A B_0 map was used as input for a second order image-based shimming routine (14 slices; slice thickness 8 mm; no slice gap; T_R/T_E 30/3.11 ms; flip angle 20°; FOV 160 × 180 mm^2).
III. T_1-weighted sequence for anatomical reference to position the 2D-CSI grid (15 slices; slice thickness 7 mm; slice gap 0.5 mm; T_R/T_E 10/3 ms; flip angle 30°; FOV 180 × 200 mm^2).

Since the boundaries between, and diameters of, individual muscles and muscle groups change along the length of the leg, the 2D-CSI grid was placed in such a way that one individual voxel was located within a single muscle over the entire length of the coil.[11]

2.4 | Data analysis

Regions of interest (ROIs) were manually drawn on the T_1-weighted images, the three-point Dixon images and the MSME images, using Medical Image Processing Analysis and Visualization (MIPAV) (https://mipav.cit.nih.gov/). Six individual lower leg muscles were segmented for this study: the lateral head of the gastrocnemius (GCL), the medial head of the gastrocnemius (GCM), the soleus (SOL), the peroneus (PER), the tibialis anterior (TA) and the tibialis posterior (TP) muscles. The MR sequences differed in parameters such as slice thickness and slice gap and therefore the number of slices used in the analysis varied between sequences, but in total covered the same ROI as the DTI. All MR outcome measures are reported as the mean value of all pixels within an ROI averaged over multiple slices.

The diffusion data-sets were analyzed using QMRITools in Mathematica (github.com/mfroeling/QMRITools). All diffusion datasets were denoised, registered and corrected for eddy current distortions and subject motion. The diffusion tensor was calculated using an iterative weighted-linear-least-squares (iWLLS) method generating three eigenvectors and the corresponding eigenvalues (λ_1, λ_2 and λ_3) per voxel. Fractional anisotropy (FA) and mean diffusivity (MD) were calculated per voxel, based on the three eigenvalues, using standard equations. The SE-DTI without diffusion weighting was used to assess SNR. SNR was calculated for each individual pixel and defined as the mean signal of the

10 dynamics divided by the SD of the same 10 dynamics. Muscles with SNR levels below 20 and fat fractions above 50% were excluded from the data analysis.[16] For the Dixon scans, fat and water images were reconstructed according to the magnitude and phase images of each of the individual echoes. Some datasets showed low signal on the third echo and there were therefore difficulties calculating the B_0. In that case, the missing B_0 points are interpolated using the surrounding points showing phase and sufficient magnitude signal on each of the echoes, after which the data were fitted to a six-peak fat model and fat fractions were calculated as [signal intensity (SI) fat/(SI fat + SI water)] × 100. For six of the healthy control subjects, raw magnitude and phase images were missing, hampering multi-peak reconstruction. Therefore, single-peak reconstruction data from the scanner software were used instead. The Dixon sequence was optimized with respect to T_R and flip angle to minimize T_1 relaxation effects. Fat fractions were not corrected for T_2^* relaxation effects. Water T_2 relaxation times were calculated using an extended phase graph (EPG) fitting approach, considering different T_2 relaxation times for a single water and a single fat component.[27] The fat T_2 relaxation time, the water T_2 relaxation time and the transmit field (B_1^+) were fitted on a voxel-by-voxel basis using a dictionary method.[28] The fat calibration was performed per subject, using 1000 pseudo-random points automatically selected from the subcutaneous fat selected from the last echo. Pseudo-random means that the points that are selected are randomly distributed through the subcutaneous fat, but if the same mask were to be applied to a particular scan in the same subject the same random voxels would be selected. Residual maps were used to visually assess the quality of the EPG fit. Pixels with a fat fraction above 50% based on the reconstructed fat fraction map were excluded from the analysis, as these pixels have been shown to impact the stability of the EPG fit.[27,28]

^{31}P MRS datasets were visualized using the 3D Interactive Chemical Shift Imaging (3diCSI) software package (https://cuit.columbia.edu/cuit/software-downloads). Phosphorus spectra were identified for the GCL, GCM, SOL, PER, TA and TP muscles, exported as free induction decays (FIDs), and processed in the time domain using AMARES in the JMRUI software package (Version 5, http://sermn02.uab.es/mrui/).[29] Voxels were carefully positioned to avoid overlap with adjoining muscles as described before.[11] If it was not possible to position a voxel wholly in a specific muscle, due to the muscle being too small, the voxel was positioned in such a way that the voxel included either air or bone (tissue from which no phosphor signal could be obtained) but no other muscle tissue. Signals from P_i, PDE, phosphocreatine (PCr) and γ-, α- and β-ATP (adenosine triphosphate) were fitted using Gaussian line shapes, and prior knowledge was used for the linewidths of the PDE and β-ATP peaks.[11] Inorganic phosphate (P_i) was modeled as a single peak. The metabolite signals were presented as a ratio over γ-ATP or PCr and corrected for T_1 saturation effects according to literature values.[30] Spectra with an SNR lower than 10 for the PCr peak and/or where not all metabolite peaks could be quantified were excluded from the analysis. SNR was determined for each of the individual spectra and defined as the amplitude of the PCr peak divided by the SD of the residual signal after fitting. No slice selection was applied in the feet-head direction during acquisition; as a result the ^{31}P MRS spectra are measured over the full length of the coil.

All muscles of the patients with BMD were classified into two groups according to their mean fat fraction: NFR and FR muscles. Cut-off values were based on the mean fat fraction + two SDs for the specific muscle in healthy controls.

2.5 | Statistical analysis

Since the qT2 and DTI data were not normally distributed, a non-parametric Kruskal-Wallis test was used to compare DTI-derived parameters and the averages and SDs of the water T_2 relaxation times between groups on a muscle-by-muscle basis. The level of statistical significance was corrected for multiple comparisons and set at $p \leq 0.0012$ (6 muscles × 7 outcome measures = 42; 0.05/42 = 0.0012). As the ^{31}P MRS data were normally distributed, a general linear model was used for the comparison of metabolite ratios between the groups for the six individual lower leg muscles. Age was entered as a covariate in the model, and level of statistical significance was corrected for multiple testing and set at $p \leq 0.0083$ (six muscles; 0.05/6 = 0.083). A post-hoc analysis was used to determine which groups differed. A Spearman correlation was used to determine the relationship between PDE levels and MD in the lower leg muscles of patients with BMD. All statistical analyses were performed in SPSS Version 24 for windows (SPSS, Chicago, IL).

3 | RESULTS

The NFR/FR BMD subgroups were defined for different muscle groups as follows: GCL n = 3/21 (cut-off fat fraction 7.3%), GCM/SOL n = 5/19 (cut-off fat fractions: 10.6%8.9%), TA n = 6/18 (cut-off fat fraction 5.3%) and PER/TP n = 7/17(cut-off fat fraction 12.0%/6.6%). For the DTI data, a total of 29 muscles (GCL 8, GCM 15, SOL 1, PER 5, TA 0, TP 0 had to be excluded due to high fat fractions. Additionally, 14 muscles had to be excluded due to insufficient SNR of the DTI (GCL 2, GCM 0, SOL 3, PER 4, TA 1, TP 4). For the average water T_2 relaxation times, a total of 16 muscles (GCL 4, GCM 7, SOL 1, PER 2, TA 1, TP 1) were excluded due to an insufficient number of pixels in the ROI to be analyzed. For the ^{31}P MRS data, a total of 27 muscles had to be excluded due to missing data (one subject), insufficient SNR or the inability to identify all metabolite peaks (GCL 4, GCM 7, SOL 4, PER 4, TA 3, TP 5). None of the healthy control muscles had to be excluded. The final numbers of subjects used for each of the analyses are visualized in Figure 1.

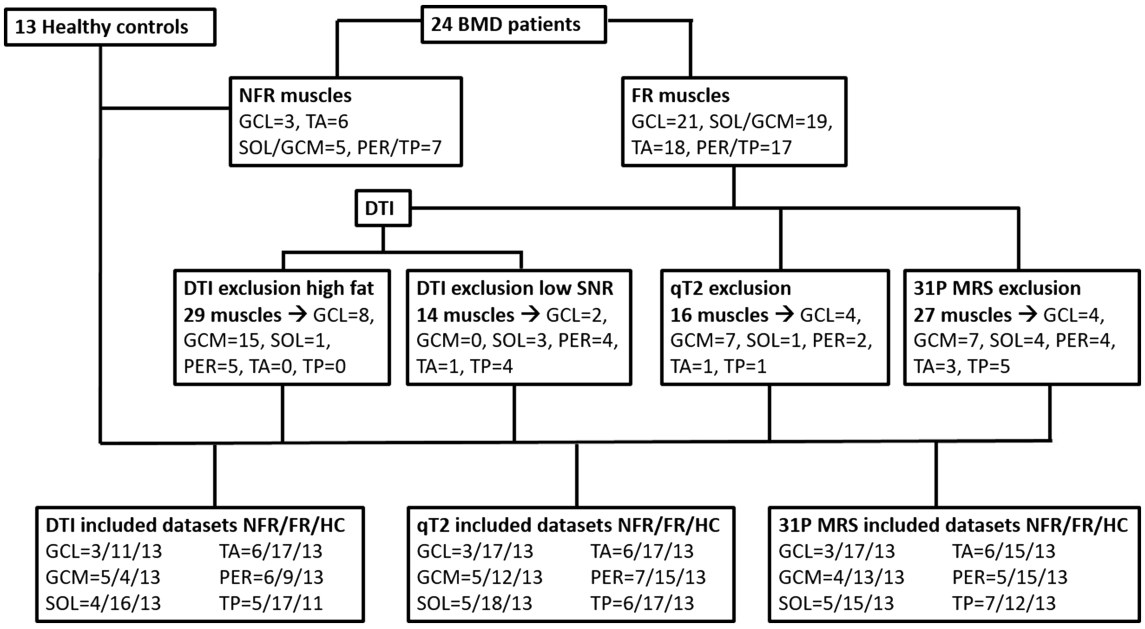

FIGURE 1 Flow diagram describing the exclusion of datasets

3.1 | Diffusion parameters

Multi-parametric axial images of a representative patient with BMD are shown in Figure 2. The means and SDs of the DTI parameters for the analyzed lower leg muscles are summarized in Table 1. No statistically significant differences were detected in diffusion indices between groups. An elevated λ_2 was seen in the FR TA muscle (p = 0.0226) compared with the NFR TA muscle (Figure 3) and an slightly elevated FA was seen in the FR SOL muscle (p = 0.03) compared with the healthy control SOL muscle, but neither reached statistical significance after correction for multiple comparisons.

3.2 | Mean and SD water T_2 relaxation times

The means and SDs of the water T_2 relaxation times for the lower leg muscles are summarized in Table 1. Representative qT2 maps, masked T_2 maps and error maps for a healthy control subject, NFR and FR patient with BMD are shown in Figure 4. Between-group analysis showed similar

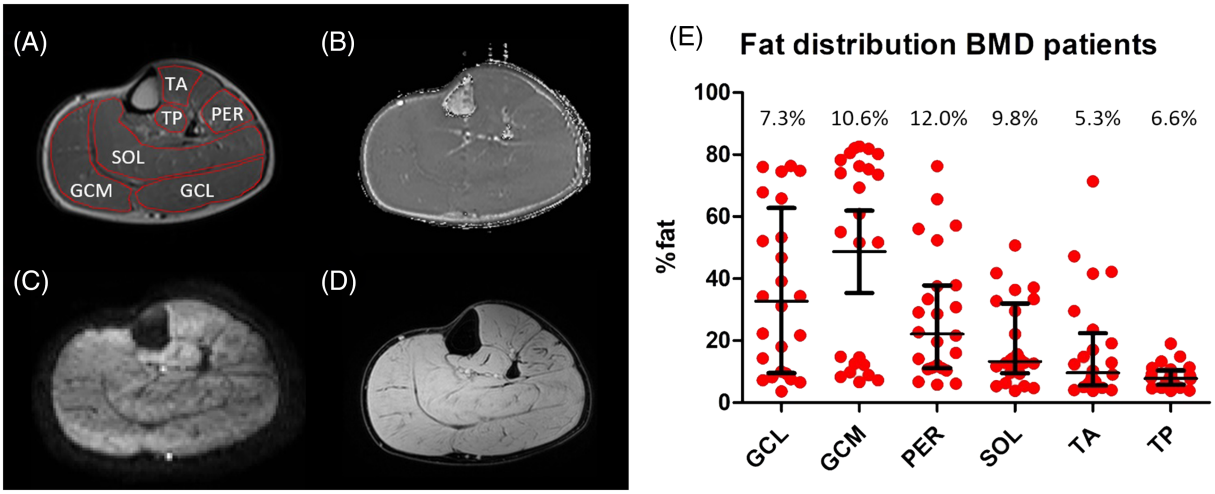

FIGURE 2 Multi-parametric axial images of the lower leg of a patient with BMD: A, first echo of a multi-SE image with ROIs for the six lower leg muscles—GCM, GCL, SOL, TA, PER and TP; B, reconstructed T_2 map using the EPG algorithm; C, SE-EPI images with diffusion weighting (b = 450 s/mm^2); D, offline reconstructed water map of the Dixon scan using six-fat-peak model; E, scatter dot plots of the mean fat fraction (% fat) with the 95% confidence interval in all patients with BMD for the GCM, GCL, PER, SOL, TA and TP muscles. The cut-off fat fractions for the individual muscles used to divide the patients with BMD into groups are reported on the graph

TABLE 1 Mean values ± SDs for the diffusion parameters and average T_2 in healthy controls, BMD muscles with NFR and BMD muscles with FR. Significant differences between patients and controls are marked with an asterisk (*)

Muscle	Parameter	NFR	FR	Healthy control
GCM		*N* = 5	*N* = 4	*N* = 13
	λ_1 (10^{-3}mm^2/s)	1.96 ± 0.06	1.97 ± 0.03	1.94 ± 0.07
	λ_2 (10^{-3}mm^2/s)	1.54 ± 0.07	1.56 ± 0.06	1.55 ± 0.05
	λ_3 (10^{-3}mm^2/s)	1.38 ± 0.05	1.39 ± 0.02	1.39 ± 0.04
	MD (10^{-3}mm^2/s)	1.63 ± 0.06	1.64 ± 0.04	1.64 ± 0.06
	FA(-)	0.18 ± 0.01	0.18 ± 0.01	0.18 ± 0.02
		N = 5	*N* = 12	*N* = 13
	T_2 (ms)	30.0 ± 1.7	28.9 ± 6.2	29.8 ± 0.8
	T_2 SD (ms)	1.0 ± 0.5	2.7 ± 1.9	0.9 ± 0.3
GCL		*N* = 3	*N* = 11	*N* = 13
	λ_1 (10^{-3}mm2/s)	2.01 ± 0.11	2.08 ± 0.11	2.02 ± 0.1
	λ_2 ((10^{-3}mm^2/s)	1.57 ± 0.11	1.68 ± 0.10	1.64 ± 0.08
	λ_3 (10^{-3}mm^2/s)	1.33 ± 0.04	1.37 ± 0.11	1.35 ± 0.05
	MD (10^{-3}mm^2/s)	1.63 ± 0.09	1.71 ± 0.1	1.67 ± 0.07
	FA (-)	0.21 ± 0.02	0.21 ± 0.02	0.20 ± 0.02
		N = 3	*N* = 17	*N* = 13
	T_2 (ms)	29.1 ± 0.7	30.6 ± 1.7	29.6 ± 1.1
	T_2 SD (ms)	0.8 ± 0.3	2.9 ± 1.9*	0.9 ± 0.2
SOL		*N* = 4	*N* = 16	*N* = 13
	λ_1 (10^{-3}mm^2/s)	2.02 ± 0.08	2.03 ± 0.08	1.99 ± 0.04
	λ_2(10^{-3}mm^2/s)	1.61 ± 0.08	1.6 ± 0.06	1.59 ± 0.04
	λ_3(10^{-3}mm^2/s)	1.38 ± 0.06	1.34 ± 0.07	1.36 ± 0.03
	MD (10^{-3}mm^2/s)	1.67 ± 0.07	1.66 ± 0.07	1.65 ± 0.03
	FA(-)	0.20 ± 0.01	0.21 ± 0.02	0.20 ± 0.01
		N = 5	*N* = 18	*N* = 13
	T_2 (ms)	30.7 ± 1.2	31.6 ± 4.0	30.2 ± 1.1
	T_2 SD (ms)	1.2 ± 0.5	3.0 ± 2.2*	1.3 ± 0.3
TA		*N* = 6	*N* = 17	*N* = 13
	λ_1 (10^{-3}mm^2/s)	2.11 ± 0.12	2.16 ± 0.08	2.17 ± 0.07
	λ_2 (10^{-3}mm^2/s)	1.58 ± 0.09	1.68 ± 0.06	1.62 ± 0.07
	λ_3 (10^{-3}mm^2/s)	1.40 ± 0.07	1.37 ± 0.08	1.40 ± 0.06
	MD (10^{-3}mm^2/s)	1.70 ± 0.08	1.74 ± 0.05	1.73 ± 0.06
	FA(-)	0.22 ± 0.02	0.23 ± 0.03	0.23 ± 0.02
		N = 6	*N* = 17	*N* = 13
	T_2 (ms)	29.3 ± 1.1	29.5 ± 1.6	29.7 ± 0.9
	T_2 SD (ms)	0.7 ± 0.3	2.0 ± 0.9*	0.7 ± 0.3
PER		*N* = 6	*N* = 9	*N* = 13
	λ_1 (10^{-3}mm^2/s)	2.02 ± 0.1	2.15 ± 0.18	2.06 ± 0.1
	λ_2 (10^{-3}mm^2/s)	1.64 ± 0.13	1.71 ± 0.1	1.68 ± 0.09
	λ_3 (10^{-3}mm^2/s)	1.33 ± 0.09	1.38 ± 0.08	1.34 ± 0.06
	MD (10^{-3}mm^2/s)	1.66 ± 0.1	1.74 ± 0.09	1.69 ± 0.07
	FA(-)	0.21 ± 0.02	0.22 ± 0.04	0.21 ± 0.03
		N = 7	*N* = 15	*N* = 13
	T_2 (ms)	28.7 ± 1.1	29.25 ± 1.7	29.1 ± 0.8
	T_2 SD (ms)	1.4 ± 0.7	2.2 ± 0.8*	1.1 ± 0.4

TABLE 1 (Continued)

Muscle	Parameter	NFR	FR	Healthy control
TP		*N* = 5	*N* = 17	*N* = 11
	λ_1 (10^{-3}mm^2/s)	2.15 ± 0.09	2.14 ± 0.1	2.12 ± 0.07
	λ_2 (10^{-3}mm^2/s)	1.6 ± 0.05	1.64 ± 0.1	1.60 ± 0.08
	λ_3 (10^{-3}mm^2/s)	1.4 ± 0.04	1.40 ± 0.08	1.36 ± 0.08
	MD (10^{-3}mm^2/s)	1.71 ± 0.05	1.72 ± 0.08	1.69 ± 0.07
	FA(-)	0.22 ± 0.03	0.2 ± 0.02	0.23 ± 0.02
		N = 6	*N* = 17	*N* = 13
	T_2 (ms)	29.1 ± 0.5	29.7 ± 2.2	29.3 ± 1.0
	T_2 SD (ms)	1.9 ± 1.4	1.9 ± 0.9	1.4 ± 0.7

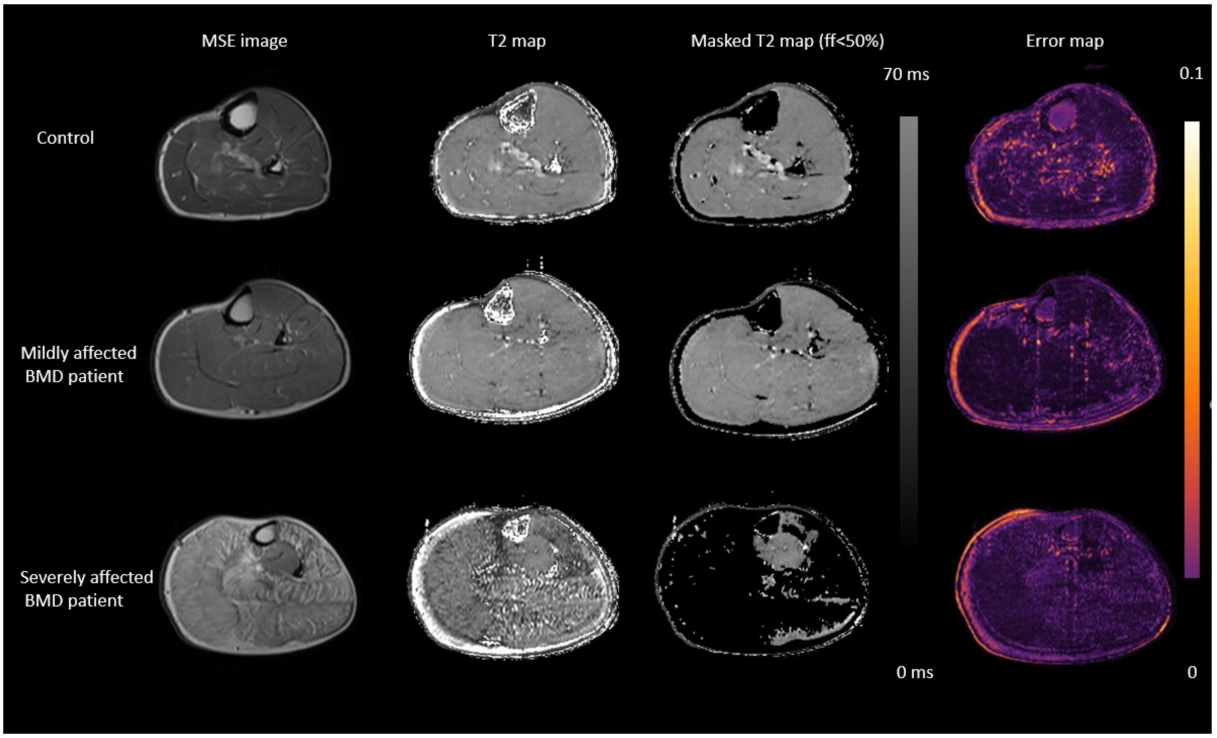

FIGURE 3 Scatter dot plots of the MD, FA and the three eigenvalues with the 95% confidence interval in healthy controls (HC), NFR BMD muscles and FR BMD muscles for the TA muscle. Significant differences between groups are indicated with asterisks (*). The other analyzed lower leg muscles showed similar findings

average water T_2 relaxation times for all groups in all lower leg muscles (Figure 5). The T_2 SD was significantly elevated for the GCL, SOL, TA and PER muscles in the FR BMD muscles compared with the control and the NFR BMD muscles ($p \leq 0.0005$) (Figure 6). The GCM ($p = 0.0064$) and TP ($p = 0.1624$) muscles showed similar patterns although they were not significantly elevated after correction for multiple comparisons (Figure 6). Error maps of the residuals of the EPG fit were homogeneous and consistent in all datasets (Figure 4).

3.3 | ^{31}P metabolite ratios

Example ^{31}P spectra of an NFR BMD muscle, an FR BMD muscle and a healthy control muscle are depicted in Figure 7. The average linewidth of the PCr signal of all subjects was 44.5 ± 21.8 Hz. Mean and SDs of the metabolic indices in the NFR and FR BMD muscles and healthy controls are shown in Table 2 and Figure 8. Compared with healthy controls, PDE levels were significantly elevated in the NFR and FR TA muscles (group effect $p = 0.008$; post-hoc FR/NFR $p = 0.005/0.035$) and FR PER (group effect $p = 0.0072$; post-hoc FR $p = 0.002$) and GCL (group effect

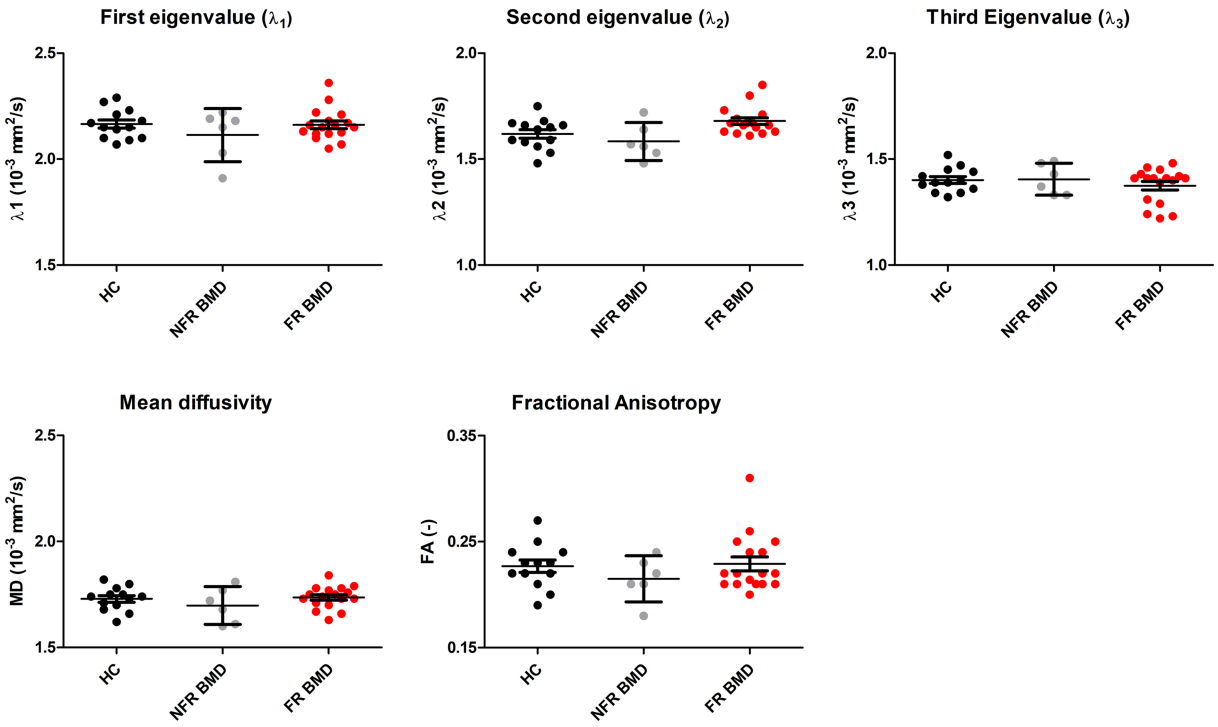

FIGURE 4 Multi-SE images, reconstructed T_2 maps using EPG fit, T_2 maps without pixels with %fat > 50% and error maps of the residual of the EPG fit are shown for the middle slice in a healthy control, a mildly affected patient with BMD and a severely affected patient with BMD. Fat fractions for the individual leg muscles in the mildly/severely affected patient with BMD were as follows: GCL 6.4/51.7%; GCM 7.7/46.9%; SOL 5.3/51.2%; PER 10.2/66.9%; TA 4.8/42.2%; TP 4.5/6.9%. Note the increase in error of the residuals near the arteries

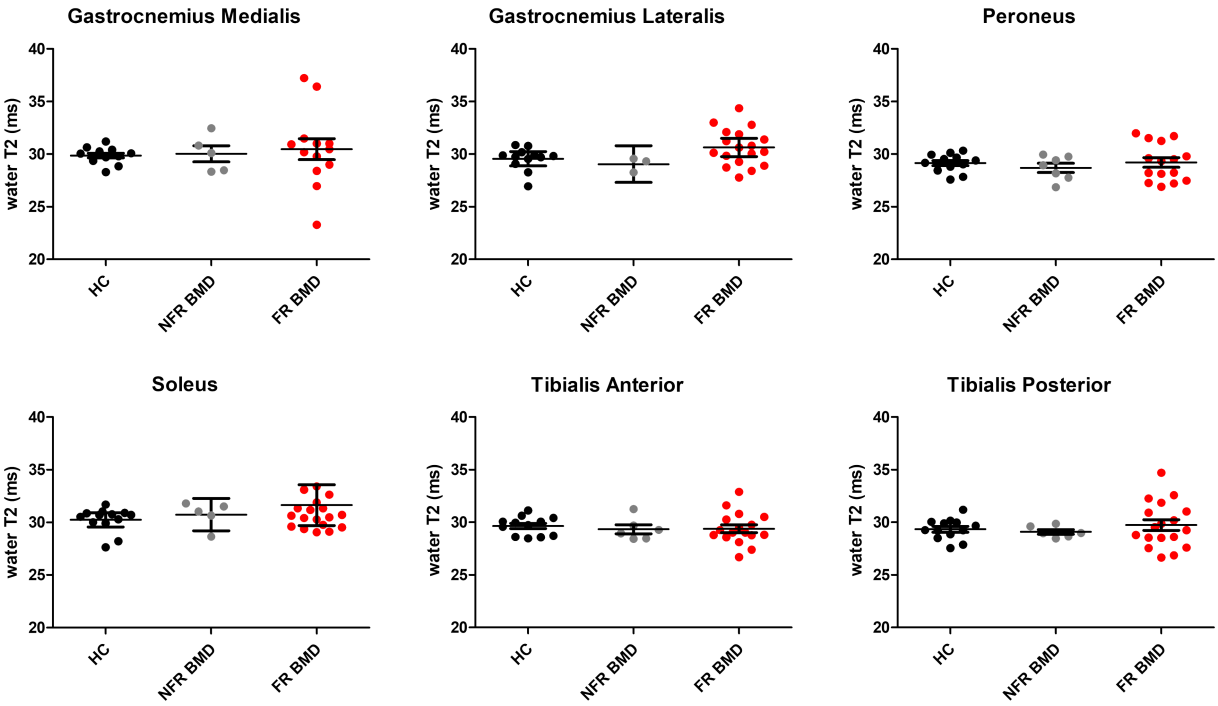

FIGURE 5 Scatter dot plots of the average water T_2 relaxation times (water T_2 (ms)) with the 95% confidence interval in healthy controls and NFR BMD muscles and FR BMD muscles for the GCM, GCL, PER, SOL, TA and TP muscles. Significant differences between groups are indicated with an asterisk (*)

p = 0.008; post-hoc FR p = 0.004) muscles. The SOL (group effect p = 0.04) muscles showed a trend for elevated PDE/ATP levels compared with healthy controls. In addition, P_i/ATP was elevated in the NFR and FR PER (group effect p = 0.003; post hoc FR/NFR p = 0.001/0.043) muscles compared with healthy control muscles. PCr/ATP was significantly higher in the NFR SOL (group effect p = 0.0002; post-hoc NFR p = 0.001)

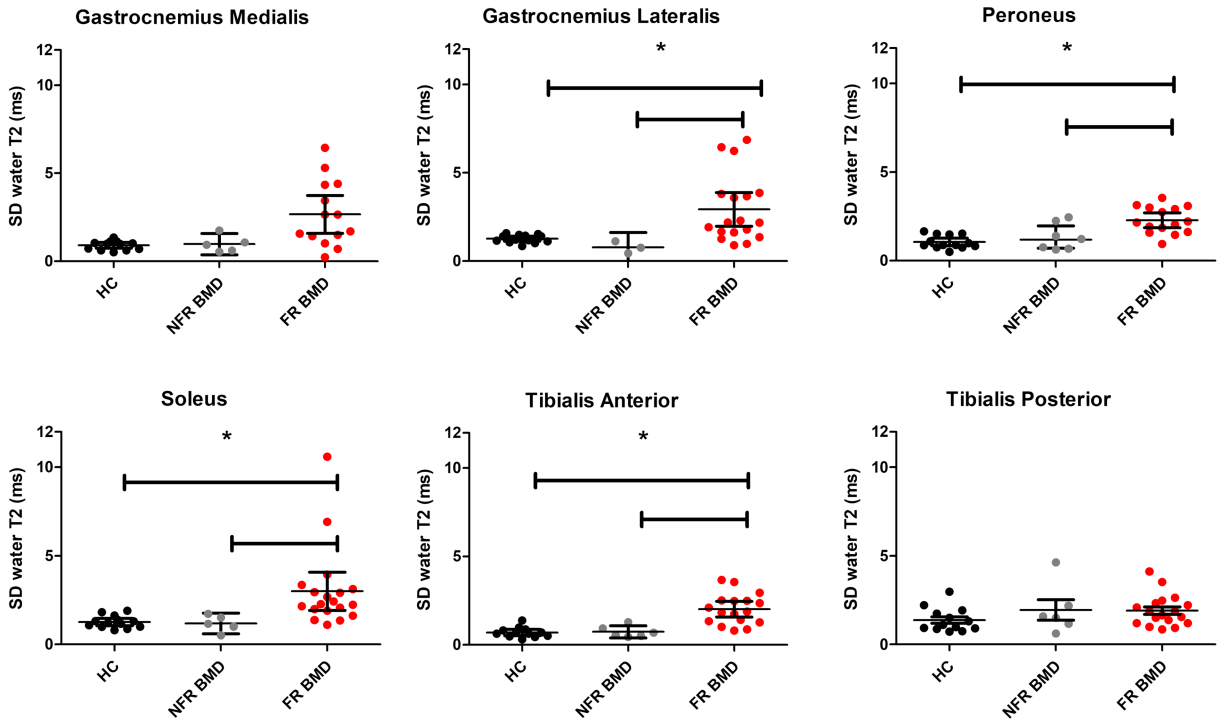

FIGURE 6 Scatter dot plots of the SD of the water T_2 relaxation times (T_2SD) with the 95% confidence interval in healthy controls and NFR BMD muscles and FR BMD muscles for the GCM, GCL, PER, SOL, TA and TP muscles. Significant differences between groups are indicated with an asterisk (*). Note the lack of change in the TP muscle, which is also the muscle with the lowest increase in %fat (see Figure 2)

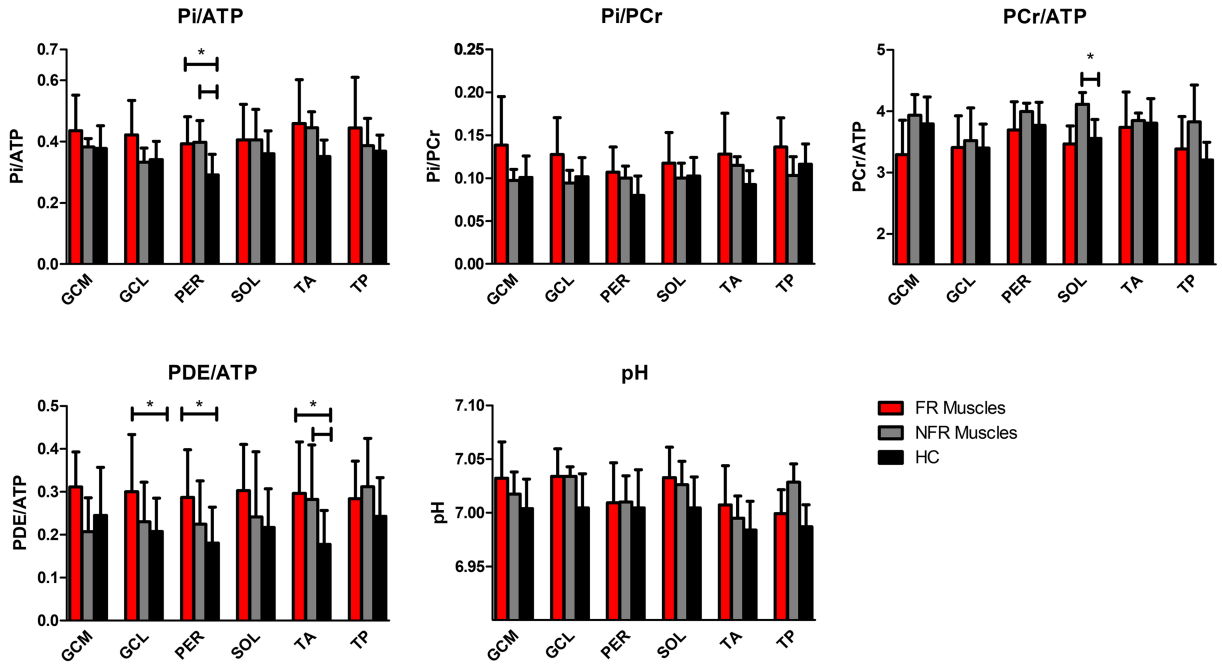

FIGURE 7 Representative ^{31}P spectrum for a muscle from a healthy control subject, an NFR muscle of a patient with BMD and an FR muscle of a patient with BMD. Note the reduction in SNR in the phosphorus spectrum of the FR BMD muscle. The spectra are scaled according to the PCr peak

muscle compared with healthy control muscles. No significant changes between groups were detected for intracellular tissue pH or P_i/PCr. However, some slight elevations in intracellular tissue pH were seen in the majority of the muscles (except PER). Additionally, a trend for elevated P_i/PCr was seen in the TA (p = 0.013) and PER (p = 0.015) muscles.

TABLE 2 Mean values ± SDs for P_i/ATP, P_i/PCr, PDE/ATP, PCr/ATP and intracellular tissue pH in healthy controls, NFR BMD muscles and FR BMD muscles. Significant differences between NFR or FR muscles and healthy controls are marked with an asterisk (*)

Muscle	Parameter	NFR	FR	Healthy control
GCM		*N* = 4	*N* = 13	*N* = 13
	P_i/ATP	0.38 ± 0.03	0.44 ± 0.12	0.38 ± 0.07
	P_i/PCr	0.1 ± 0.01	0.14 ± 0.06	0.10 ± 0.03
	PDE/ATP	0.21 ± 0.08	0.31 ± 0.08	0.25 ± 0.11
	PCr/ATP	3.93 ± 0.34	3.29 ± 0.56	3.8 ± 0.44
	pH	7.02 ± 0.02	7.03 ± 0.03	7.00 ± 0.03
GCL		*N* = 3	*N* = 17	*N* = 13
	P_i/ATP	0.35 ± 0.05	0.41 ± 0.11	0.34 ± 0.06
	P_i/PCr	0.1 ± 0.02	0.12 ± 0.04	0.1 ± 0.02
	PDE/ATP	0.17 ± 0.05	0.30 ± 0.12*	0.21 ± 0.07
	PCr/ATP	3.48 ± 0.53	3.431 ± 0.52	3.40 ± 0.4
	pH	7.03 ± 0.01	7.03 ± 0.02	7.00 ± 0.03
SOL		*N* = 5	*N* = 15	*N* = 13
	P_i/ATP	0.41 ± 0.1	0.41 ± 0.1	0.36 ± 0.08
	P_i/PCr	0.1 ± 0.02	0.12 ± 0.04	0.10 ± 0.02
	PDE/ATP	0.24 ± 0.15	0.30 ± 0.11	0.22 ± 0.09
	PCr/ATP	4.12 ± 0.19*	3.47 ± 0.3	3.56 ± 0.31
	pH	7.03 ± 0.02	7.03 ± 0.03	7.00 ± 0.03
TA		*N* = 6	*N* = 15	*N* = 13
	P_i/ATP	0.45 ± 0.05	0.46 ± 0.15	0.35 ± 0.05
	P_i/PCr	0.11 ± 0.01	0.13 ± 0.05	0.09 ± 0.01
	PDE/ATP	0.29 ± 0.10*	0.30 ± 0.12*	0.18 ± 0.08
	PCr/ATP	4.05 ± 0.33	3.65 ± 0.6	3.81 ± 0.4
	pH	7.00 ± 0.02	7.01 ± 0.04	6.98 ± 0.03
PER		*N* = 5	*N* = 15	*N* = 13
	P_i/ATP	0.39 ± 0.06*	0.40 ± 0.09*	0.29 ± 0.07
	P_i/PCr	0.1 ± 0.014	0.11 ± 0.03	0.08 ± 0.02
	PDE/ATP	0.23 ± 0.09	0.29 ± 0.11*	0.18 ± 0.08
	PCr/ATP	4.05 ± 0.17	3.66 ± 0.45	3.77 ± 0.4
	Ph	7.01 ± 0.02	7.01 ± 0.04	7.00 ± 0.04
TP		*N* = 7	*N* = 12	*N* = 13
	P_i/ATP	0.38 ± 0.09	0.45 ± 0.16	0.37 ± 0.05
	P_i/PCr	0.12 ± 0.03	0.13 ± 0.04	0.12 ± 0.02
	PDE/ATP	0.26 ± 0.11	0.31 ± 0.08	0.24 ± 0.09
	PCr/ATP	3.55 ± 0.56	3.5 ± 0.61	3.20 ± 0.29
	pH	7.01 ± 0.02	7.01 ± 0.03	6.99 ± 0.02

3.4 | PDE levels in relation to MD

None of the muscles (Spearman *r*; GCM 0.27; GCL 0.25; PER 0.23; SOL 0.06; TA 0.12; TP 0.06) showed a significant correlation between PDE levels and MD.

4 | DISCUSSION

In this study we evaluated diffusion measures, water T_2 relaxation times and ^{31}P metabolites as potential early markers for muscle tissue changes in patients with BMD. Our results showed that PDE levels were significantly increased in NFR TA and FR TA, PER and GCL muscles, while T_2

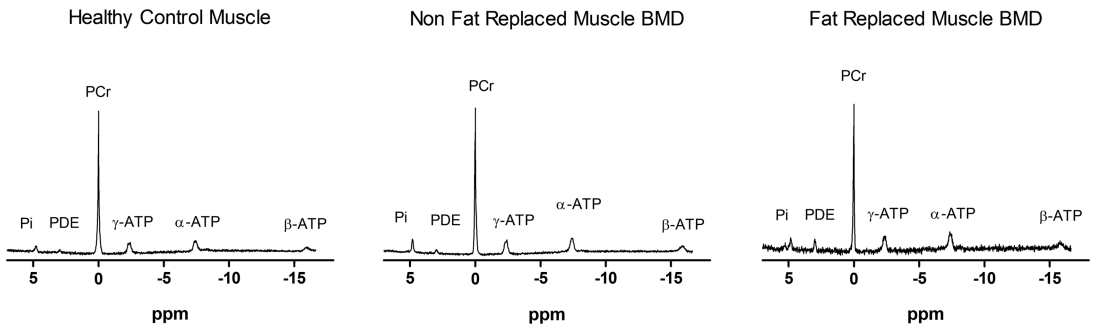

FIGURE 8 Mean values ± SDs for P_i/ATP, P_i/PCr, PCr/ATP, PDE/ATP and intracellular tissue pH in healthy control muscles, NFR BMD muscles and FR BMD muscles for each muscle. Significant differences between NFR and FR BMD muscles and controls are marked with an asterisk (*)

heterogeneity was significantly increased in the majority of lower leg muscles of the FR group. No changes were found for the DTI indices. This indicates that primarily muscles that are further along in the disease process, as defined by elevated fat fractions, showed changes in T_2 heterogeneity and ^{31}P metabolites.

4.1 | DTI parameters

The mean diffusion values in the lower leg muscles of our healthy control subjects were in agreement with other diffusion studies performed in the lower leg muscles.[31,32] With the current sample size and acquisition methods, and after excluding datasets with low SNR levels and high fat percentages (>50%), no consistent changes were detected in diffusion parameters between the groups. This is in agreement with previous work in patients with DMD, in which also no clear changes in diffusion properties were detected compared with healthy controls.[16] However, from muscle biopsy studies in patients with BMD, it is known that there are prominent changes in muscle fiber size and fiber dimensions compared with healthy muscle tissue.[33] Consequently, the similar diffusion properties between the groups found here suggest that the expected changes in muscle microstructure cannot be detected by the SE-DTI technique. This is most likely partly related to the restricted sensitivity of the SE-DTI technique caused by the use of short diffusion times, which are limited by the short T_2 relaxation times of skeletal muscle, in combination with the size of a muscle cell. Stimulated echo DTI approaches do allow for the use of longer mixing times, as the magnetization is stored in the longitudinal plane, which results in the diffusion weighting being dependent on the T_1 relaxation time of muscle, which is much longer than the T_2 value. Preclinical work used such a stimulated echo diffusion measurement approach in combination with a random permeability model in mdx mice, and found microstructural changes in skeletal muscle compared with controls and throughout the time course of the disease.[34] Therefore, for future work it would be highly interesting to assess muscle diffusion properties with these longer mixing times in patients with BMD.

4.2 | Mean and SD water T_2 relaxation times

4.2.1 | Mean water T_2 relaxation times

No significant changes were detected in average water T_2 relaxation times in any of the lower leg muscles of patients with BMD compared with healthy controls. These findings are in agreement with previous work assessing muscle inflammation in patients with BMD using fat-suppressed T_2 measurements in the lower leg muscles.[22] However, recently presented work in a large BMD cohort (n = 86) did show a very small (0.8 ms) but significant increase in average water T_2 values in the upper leg muscles compared with healthy age-matched controls using a sequence similar to that used here.[23] This suggests that there could be a very small inflammatory component present in the muscles of patients with BMD. This would be in line with muscle biopsy studies, showing that inflammatory cells are more prominently present in patients with DMD compared with patients with BMD.[33] In the literature, abnormalities of the water T_2 component have been associated with a wide variety of processes such as membrane leakage, fibrosis and inflammation.[35–37] The impact of these processes combined has been introduced as "disease activity" and is thought to reflect the intensity of underlying pathophysiological changes.[37] However, recent work showed a negative dependency of water T_2 values measured with single-voxel ^{1}H MRS and fat fraction, indicating that fat replacement itself might have an effect on water T_2 independent of the acquisition method used.[38] As many individual processes are known to act alongside one another in muscle diseases while having opposing effects on water T_2 relaxation times, water T_2 as an outcome measure is not very specific. This in combination with a possibly very small inflammatory component in BMD may explain not finding any differences in average water T_2 relaxation times in this study.

4.2.2 | SD of the T_2 relaxation times

We observed an increased T_2 heterogeneity in the majority of the FR lower leg muscles but not in NFR muscles. This suggests that the increase in T_2 heterogeneity only occurs in later stages of the disease, as defined by the increased fat fraction. To our knowledge this is the first study measuring T_2 heterogeneity in patients with BMD in relation to the disease course. Previous work also showed an increased water T_2 SD in patients with BMD compared with controls, which is in agreement with our findings.[23] A similar phenomenon has been previously reported in Golden Retriever muscular dystrophy (GRMD) dogs, where an increase in T_2 heterogeneity was able to differentiate GRMD muscles from healthy ones independent of the age of the dog.[21] Interpretation of changes in T_2 heterogeneity is complex, as not only pathophysiological but also methodological factors such as fit instabilities, low SNR and fat fraction are known to increase the SD.[28] The homogeneous error maps of the residuals of the fit across the groups in combination with only using pixels with fat fraction below 50% rules out some of these methodological factors in this study. This suggests that the increased T_2 heterogeneity detected in the FR muscles of patients with BMD could be related to an increased disease activity. The detection of these small inflammatory regions in the muscles of patients with BMD is especially challenging when using a whole muscle analysis. Other measures (eg smaller regions of interest) or analysis methods (eg histogram analysis) need to be explored to evaluate the presence of these small inflammatory regions.

4.3 | ^{31}P metabolic indices

In skeletal muscle, ^{31}P metabolic indices are predominantly present in the muscle tissue but not in the fat tissue. Consequently, ^{31}P metabolic indices are not only of interest in the absence of fat but can also reflect changes in muscle tissue itself in later stages of the diseases. In this study, PDE levels were significantly elevated in the NFR TA and FR TA, PER and GCL muscles compared with control muscles. Despite the lack of significant changes in PDE levels in the majority of NFR muscles and some of the FR muscles compared with controls, our results partly reflect a similar phenomenon as previously described in patients with BMD and DMD.[11,12,39] This variation in PDE levels between the lower leg muscles and across studies could be caused by the varying rates in disease progression between individual muscles and the low number of subjects and highly heterogeneous early disease phase in the NFR BMD group. However, this increase in PDE levels, generally attributed to membrane degradation products in muscular dystrophies, reflects changes in muscle tissue without, and in the presence of, fat replacement in patients with BMD. Interestingly, in recent studies in type II diabetes, increased PDE levels have been associated with mitochondrial dysfunction and abnormalities in insulin signaling.[40] The role of these processes in muscular dystrophies is unknown, but could have made a contribution to the signal increase we detected here. Other metabolic indices were changed in muscles further along in the disease process, as demonstrated by the increased fat fraction. The P_i/PCr ratio showed a slight increase in the FR TA and PER muscles, although not significantly after correction for multiple comparisons. An increased P_i/PCr ratio is often linked to elevated ADP concentrations due to poor coupling of the oxidative phosphorylation in resting skeletal muscle.[41–45] Interestingly, recent studies showed splitting of the P_i peak into P_{ia} and P_{ib} (0.3 ppm resonance downfield from P_{ia}) peaks in GRMD dogs and in patients with DMD with both P_i peaks being elevated compared with controls.[46,47] The P_{ia} peak is thought to correspond to a physiological intracellular pH while the P_{ib} peak is thought to originate from degenerating hypercontracted cells with inadequate pH homeostasis. The P_{ib} peak is therefore considered to be more specific to dystrophic processes and could potentially be the underlying cause of the increased P_i/PCr ratio. This splitting of the P_i peak into P_{ia} and P_{ib} was not visible in our data. The exact reason for this is not fully clear but is likely related to lower SNR in our dataset compared with articles where this splitting was reported. We used a volume coil with a diameter of about 20 cm, and 2D CSI acquisition with 24 NSA, while the previously reported data were acquired using surface coil localized measurements with small surface coils.[46–48] Moreover, the greater line widths (44.5 ± 21.8 Hz) of the PCr peak in our data compared with these previous studies (range of PCr line widths 17-35 Hz) could have resulted in not detecting this splitting of the P_i peak.[46–48] No clear changes were found for the intracellular tissue pH between the groups. However, some of the muscles (SOL, GCL and TP) showed a trend for a more alkaline intracellular tissue pH compared with controls. This pattern would be in accordance with previous work in mild to moderately affected patients with BMD.[45,49] Multiple processes are thought to be involved with the more alkaline intracellular tissue pH in muscular dystrophies, ie mitogenesis, as muscle tissue is continuously regenerating, the enhanced alkaline P_{ib} originating from degenerating hypercontracted cells and an altered proton sarcolemma efflux mechanism induced by a misbalance in Ca^+.[36,41,46,50] Only minor changes were found for the other metabolite ratios (P_i/ATP and PCr/ATP). This is in agreement with previous surface coil and spatially localized work pointing out that energy metabolism only becomes increasingly misbalanced in later disease stages, showing clear increases in P_i/ATP and decreases in PCr/ATP ratios.[11,41,43–45] Additionally, these changes in metabolite ratios in BMD show a similar pattern as in DMD but a little less pronounced.

4.4 | Relation between PDE levels and mMD

Both PDE levels and DTI parameters have been associated with membrane integrity in skeletal muscles.[13,24,25] In this study, we explored the relation between PDE levels and MD in the muscles of patients with BMD for the first time, but did not observe any correlation. This could be due to

multiple factors. To start with, no clear changes were detected in any of the DTI parameters in the muscles of patients with BMD compared with controls, which resulted in a small dynamic range. Another cause could be that the two outcome measures reflect different parts of membrane integrity. Differences in PDE levels have also been associated with changes in energy metabolism, specifically mitochondrial dysfunction and abnormalities in insulin signaling in patients with Type II diabetes.[40] The role of these processes in muscular dystrophies is unclear, but could have contributed to not finding a correlation. In future work it would be interesting to assess this in a larger cohort of patients with BMD and in patients with other muscular dystrophies, as well as exploring a stimulated echo approach for DTI.

4.5 | Limitations

Some limitations of the study should be acknowledged. First of all, as mentioned above, some of the diffusion tensor images (19%), T2 datasets (7%) and ^{31}P spectra (12%) had to be discarded due to insufficient quality as a result of extensive fat replacement. This could have resulted in some bias towards less severely affected muscles and could possibly explain why no significant abnormalities were found in diffusion measures, average water T_2 relaxation times or some of the metabolic indices in the FR muscles. Second, the number of patients in the NFR group of muscles was relatively low compared with the FR group and healthy controls, and this might have influenced the findings in this study. This tendency is clearly visualized in the metabolic indices and as a result may underestimate the metabolic changes in NFR BMD muscles. However, no consistent pattern was observed for the DTI parameters or average water T_2 values across the NFR muscles. A more general point is the highly heterogeneous disease course in BMD, most evident in the FR muscles of the patients with BMD. This heterogeneity in disease stages within the group as well as the heterogeneity within individual muscles results in a large SD. This complicates the interpretation of the results in the FR BMD muscle group.

5 | CONCLUSION

In conclusion, our results indicate that primarily muscles that are further along in the disease process showed changes in T_2 heterogeneity and ^{31}P metabolic indices between groups. No clear changes were found for the DTI indices between groups.

ACKNOWLEDGEMENTS

The authors thank Celine Baligand for discussing the manuscript.

The authors are members of the European Reference Network for Rare Neuromuscular Diseases (ERN EURO-NMD).

ORCID

Melissa T. Hooijmans https://orcid.org/0000-0002-2233-1383
Martijn Froeling https://orcid.org/0000-0003-3841-0497
Andrew Webb https://orcid.org/0000-0003-4045-9732
Hermien E. Kan https://orcid.org/0000-0002-5772-7177

REFERENCES

1. Hoffman EP, Brown RH Jr, Kunkel LM. Dystrophin: the protein product of the Duchenne muscular dystrophy locus. *Cell*. 1987;51(6):919-928. https://doi.org/10.1016/0092-8674(87)90579-4
2. Petrof BJ, Shrager JB, Stedman HH, Kelly AM, Sweeney HL. Dystrophin protects the sarcolemma from stresses developed during muscle contraction. *Proc Natl Acad Sci U S A*. 1993;90(8):3710-3714. https://doi.org/10.1073/pnas.90.8.3710
3. McDouall RM, Dunn MJ, Dubowitz V. Nature of the mononuclear infiltrate and the mechanism of muscle damage in juvenile dermatomyositis and Duchenne muscular dystrophy. *J Neurol Sci*. 1990;99(2/3):199-217. https://doi.org/10.1016/0022-510x(90)90156-h
4. Willcocks RJ, Rooney WD, Triplett WT, et al. Multicenter prospective longitudinal study of magnetic resonance biomarkers in a large Duchenne muscular dystrophy cohort. *Ann Neurol*. 2016;79(4):535-547. https://doi.org/10.1002/ana.24599
5. Janssen BH, Voet NB, Nabuurs CI, et al. Distinct disease phases in muscles of facioscapulohumeral dystrophy patients identified by MR detected fat infiltration. *PLoS ONE*. 2014;9(1):e85416. https://doi.org/10.1371/journal.pone.0085416
6. Tasca G, Iannaccone E, Monforte M, et al. Muscle MRI in Becker muscular dystrophy. *Neuromuscul Disord*. 2012;22(Suppl 2):S100-S106. https://doi.org/10.1016/j.nmd.2012.05.015
7. Lokken N, Hedermann G, Thomsen C, Vissing J. Contractile properties are disrupted in Becker muscular dystrophy, but not in limb girdle type 2I. *Ann Neurol*. 2016;80(3):466-471. https://doi.org/10.1002/ana.24743
8. Monforte M, Mercuri E, Laschena F, Ricci E, Tasca G. Calf muscle involvement in Becker muscular dystrophy: when size does not matter. *J Neurol Sci*. 2014;347(1/2):301-304. https://doi.org/10.1016/j.jns.2014.10.030
9. Fischer D, Hafner P, Rubino D, et al. The 6-minute walk test, motor function measure and quantitative thigh muscle MRI in Becker muscular dystrophy: a cross-sectional study. *Neuromuscul Disord*. 2016;26(7):414-422. https://doi.org/10.1016/j.nmd.2016.04.009

10. Wokke BH, van den Bergen JC, Versluis MJ, et al. Quantitative MRI and strength measurements in the assessment of muscle quality in Duchenne muscular dystrophy. *Neuromuscul Disord*. 2014;24(5):409-416. https://doi.org/10.1016/j.nmd.2014.01.015
11. Wokke BH, Hooijmans MT, van den Bergen JC, Webb AG, Verschuuren JJ, Kan HE. Muscle MRS detects elevated PDE/ATP ratios prior to fatty infiltration in Becker muscular dystrophy. *NMR Biomed*. 2014;27(11):1371-1377. https://doi.org/10.1002/nbm.3199
12. Hooijmans MT, Niks EH, Burakiewicz J, Verschuuren JJGM, Webb AG, Kan HE. Elevated phosphodiester and T2 levels can be measured in the absence of fat infiltration in Duchenne muscular dystrophy patients. *NMR in Biomedicine*. 2017;30(1):e3667. https://doi.org/10.1002/nbm.3667
13. Zaraiskaya T, Kumbhare D, Noseworthy MD. Diffusion tensor imaging in evaluation of human skeletal muscle injury. *J Magn Reson Imaging*. 2006;24(2):402-408. https://doi.org/10.1002/jmri.20651
14. Froeling M, Oudeman J, Strijkers GJ, et al. Muscle changes detected with diffusion-tensor imaging after long-distance running. *Radiology*. 2015;274(2):548-562. https://doi.org/10.1148/radiol.14140702
15. Williams SE, Heemskerk AM, Welch EB, Li K, Damon BM, Park JH. Quantitative effects of inclusion of fat on muscle diffusion tensor MRI measurements. *J Magn Reson Imaging*. 2013;38(5):1292-1297. https://doi.org/10.1002/jmri.24045
16. Hooijmans MT, Damon BM, Froeling M, et al. Evaluation of skeletal muscle DTI in patients with duchenne muscular dystrophy. *NMR Biomed*. 2015;28(11):1589-1597. https://doi.org/10.1002/nbm.3427
17. Froeling M, Nederveen AJ, Nicolay K, Strijkers GJ. DTI of human skeletal muscle: the effects of diffusion encoding parameters, signal-to-noise ratio and T_2 on tensor indices and fiber tracts. *NMR Biomed*. 2013;26(11):1339-1352. https://doi.org/10.1002/nbm.2959
18. Damon BM. Effects of image noise in muscle diffusion tensor (DT)-MRI assessed using numerical simulations. *Magn Reson Med*. 2008;60(4):934-944. https://doi.org/10.1002/mrm.21707
19. Burakiewicz J, Hooijmans MT, Webb AG, Verschuuren J, Niks EH, Kan HE. Improved olefinic fat suppression in skeletal muscle DTI using a magnitude-based Dixon method. *Magn Reson Med*. 2018;79(1):152-159. https://doi.org/10.1002/mrm.26655
20. Willcocks RJ, Arpan IA, Forbes SC, et al. Longitudinal measurements of MRI-T_2 in boys with Duchenne muscular dystrophy: effects of age and disease progression. *Neuromuscul Disord*. 2014;24(5):393-401. https://doi.org/10.1016/j.nmd.2013.12.012
21. Thibaud JL, Azzabou N, Barthelemy I, et al. Comprehensive longitudinal characterization of canine muscular dystrophy by serial NMR imaging of GRMD dogs. *Neuromuscul Disord*. 2012;22(Suppl 2):S85-S99. https://doi.org/10.1016/j.nmd.2012.05.010
22. Wokke BH, Van Den Bergen JC, Hooijmans MT, Verschuuren JJ, Niks EH, Kan HE. T2 relaxation times are increased in skeletal muscle of DMD but not BMD patients. *Muscle Nerve*. 2016;53(1):38-43. https://doi.org/10.1002/mus.24679
23. Marty B, Toussaint M, Gilles R, Wahbi K, Carlier P. Skeletal muscle tissue characterization of a large cohort of patients with Becker muscular dystrophy using quantitative NMR imaging. *Neuromuscul Disord*. 2017;27:S126-S126. https://doi.org/10.1016/j.nmd.2017.06.125
24. Burt CT, Glonek T, Barany M. Phosphorus-31 nuclear magnetic resonance detection of unexpected phosphodiesters in muscle. *Biochemistry*. 1976;15(22):4850-4853. https://doi.org/10.1021/bi00667a015
25. Satrustegui J, Berkowitz H, Boden B, et al. An in vivo phosphorus nuclear magnetic resonance study of the variations with age in the phosphodiester content of human muscle. *Mech Ageing Dev*. 1988;42(2):105-114. https://doi.org/10.1016/0047-6374(88)90066-8
26. van den Bergen JC, Ginjaar HB, van Essen AJ, et al. Forty-five years of Duchenne muscular dystrophy in The Netherlands. *J Neuromuscul Dis*. 2014;1(1):99-109.
27. Marty B, Baudin PY, Reyngoudt H, et al. Simultaneous muscle water T_2 and fat fraction mapping using transverse relaxometry with stimulated echo compensation. *NMR Biomed*. 2016;29(4):431-443. https://doi.org/10.1002/nbm.3459
28. Keene KR, Beenakker JM, Hooijmans MT, et al. T_2 relaxation-time mapping in healthy and diseased skeletal muscle using extended phase graph algorithms. *Magn Reson Med*. 2020. https://doi.org/10.1002/mrm.28290
29. Naressi A, Couturier C, Castang I, de Beer R, Graveron-Demilly D. Java-based graphical user interface for MRUI, a software package for quantitation of in vivo/medical magnetic resonance spectroscopy signals. *Comput Biol Med*. 2001;31(4):269-286. https://doi.org/10.1016/s0010-4825(01)00006-3
30. Bogner W, Chmelik M, Schmid AI, Moser E, Trattnig S, Gruber S. Assessment of ^{31}P relaxation times in the human calf muscle: a comparison between 3 T and 7 T in vivo. *Magn Reson Med*. 2009;62(3):574-582. https://doi.org/10.1002/mrm.22057
31. Schlaffke L, Rehmann R, Rohm M, et al. Multi-center evaluation of stability and reproducibility of quantitative MRI measures in healthy calf muscles. *NMR Biomed*. 2019;32(9):e4119. https://doi.org/10.1002/nbm.4119
32. Rockel C, Noseworthy MD. An exploration of diffusion tensor eigenvector variability within human calf muscles. *J Magn Reson Imaging*. 2016;43(1):190-202. https://doi.org/10.1002/jmri.24957
33. Dennett X, Shield LK, Clingan LJ, Woolley DA. Becker and Duchenne muscular dystrophy: a comparative morphological study. *Aust Paediatr J*. 1988;24(Suppl 1):15-20.
34. Winters KV, Reynaud O, Novikov DS, Fieremans E, Kim SG. Quantifying myofiber integrity using diffusion MRI and random permeable barrier modeling in skeletal muscle growth and Duchenne muscular dystrophy model in mice. *Magn Reson Med*. 2018;80(5):2094-2108. https://doi.org/10.1002/mrm.27188
35. Arpan I, Willcocks RJ, Forbes SC, et al. Examination of effects of corticosteroids on skeletal muscles of boys with DMD using MRI and MRS. *Neurology*. 2014;83(11):974-980. https://doi.org/10.1212/WNL.0000000000000775
36. Hogrel JY, Wary C, Moraux A, et al. Longitudinal functional and NMR assessment of upper limbs in Duchenne muscular dystrophy. *Neurology*. 2016;86(11):1022-1030. https://doi.org/10.1212/WNL.0000000000002464
37. Carlier PG. Global T2 versus water T2 in NMR imaging of fatty infiltrated muscles: different methodology, different information and different implications. *Neuromuscul Disord*. 2014;24(5):390-392. https://doi.org/10.1016/j.nmd.2014.02.009
38. Schlaeger S, Weidlich D, Klupp E, et al. Decreased water T_2 in fatty infiltrated skeletal muscles of patients with neuromuscular diseases. *NMR Biomed*. 2019;32(8):e4111. https://doi.org/10.1002/nbm.4111
39. Hooijmans MT, Doorenweerd N, Baligand C, et al. Spatially localized phosphorous metabolism of skeletal muscle in Duchenne muscular dystrophy patients: 24-month follow-up. *PLoS ONE*. 2017;12(8):e0182086. https://doi.org/10.1371/journal.pone.0182086
40. Szendroedi J, Schmid AI, Chmelik M, et al. Skeletal muscle phosphodiester content relates to body mass and glycemic control. *PLoS ONE*. 2011;6(7):e21846. https://doi.org/10.1371/journal.pone.0021846

41. Kemp GJ, Taylor DJ, Dunn JF, Frostick SP, Radda GK. Cellular energetics of dystrophic muscle. *J Neurol Sci*. 1993;116(2):201-206. https://doi.org/10.1016/0022-510x(93)90326-t
42. Younkin DP, Berman P, Sladky J, Chee C, Bank W, Chance B. ^{31}P NMR studies in Duchenne muscular dystrophy: age-related metabolic changes. *Neurology*. 1987;37(1):165-169. https://doi.org/10.1212/wnl.37.1.165
43. Barbiroli B, Funicello R, Iotti S, Montagna P, Ferlini A, Zaniol P. ^{31}P-NMR spectroscopy of skeletal muscle in Becker dystrophy and DMD/BMD carriers. Altered rate of phosphate transport. *J Neurol Sci*. 1992;109(2):188-195. https://doi.org/10.1016/0022-510x(92)90167-j
44. Newman RJ. An in vivo study of muscle phosphate metabolism in Becker's dystrophy by ^{31}P NMR spectroscopy. *Metabolism*. 1985;34(8):737-740. https://doi.org/10.1016/0026-0495(85)90024-1
45. Tosetti M, Linsalata S, Battini R, et al. Muscle metabolic alterations assessed by 31-phosphorus magnetic resonance spectroscopy in mild Becker muscular dystrophy. *Muscle Nerve*. 2011;44(5):816-819. https://doi.org/10.1002/mus.22181
46. Wary C, Naulet T, Thibaud JL, Monnet A, Blot S, Carlier PG. Splitting of Pi and other ^{31}P NMR anomalies of skeletal muscle metabolites in canine muscular dystrophy. *NMR Biomed*. 2012;25(10):1160-1169. https://doi.org/10.1002/nbm.2785
47. Wary C, Azzabou N, Giraudeau C, et al. Quantitative NMRI and NMRS identify augmented disease progression after loss of ambulation in forearms of boys with Duchenne muscular dystrophy. *NMR Biomed*. 2015;28(9):1150-1162. https://doi.org/10.1002/nbm.3352
48. Kan HE, Klomp DW, Wong CS, et al. *In vivo* ^{31}P MRS detection of an alkaline inorganic phosphate pool with short T1 in human resting skeletal muscle. *NMR Biomed*. 2010;23(8):995-1000. https://doi.org/10.1002/nbm.1517
49. Lodi R, Kemp GJ, Muntoni F, et al. Reduced cytosolic acidification during exercise suggests defective glycolytic activity in skeletal muscle of patients with Becker muscular dystrophy. An *in vivo* ^{31}P magnetic resonance spectroscopy study. *Brain*. 1999;122(Pt 1):121-130. https://doi.org/10.1093/brain/122.1.121
50. Argov Z, Lofberg M, Arnold DL. Insights into muscle diseases gained by phosphorus magnetic resonance spectroscopy. *Muscle Nerve*. 2000;23(9):1316-1334. https://doi.org/10.1002/1097-4598(200009)23:9<1316::aid-mus2>3.0.co;2-i

How to cite this article: Hooijmans MT, Froeling M, Koeks Z, et al. Multi-parametric MR in Becker muscular dystrophy patients. *NMR in Biomedicine*. 2020;33:e4385. https://doi.org/10.1002/nbm.4385